O_2 reduction by a functional heme/nonheme bis-iron NOR model complex

James P. Collman[1], Abhishek Dey, Ying Yang, Somdatta Ghosh, and Richard A. Decréau

Department of Chemistry, Stanford University, Stanford, CA 94305

Contributed by James P. Collman, April 28, 2009 (sent for review February 24, 2009)

O_2 reactivity of a functional NOR model is investigated by using electrochemistry and spectroscopy. The electrochemical measurements using interdigitated electrodes show very high selectivity for 4e O_2 reduction with minimal production of partially reduced oxygen species (PROS) under both fast and slow electron flux. Intermediates trapped at cryogenic temperatures and characterized by using resonance Raman spectroscopy under single-turnover conditions indicate that an initial bridging peroxide intermediate undergoes homolytic O—O bond cleavage generating a *trans* heme/nonheme bis-ferryl intermediate. This bis ferryl species can oxygenate 2 equivalents of a reactive substrate.

electrochemistry | ferryl | NOR functional model | O_2 reductase | PROS

Cytochrome *c* oxidase (CcO) and nitric oxide reductase (NOR) belong to the heme copper oxidase superfamily of enzymes (1, 2). CcO is the terminal enzyme in the respiratory chain of higher organisms, located in their mitochondrial membrane, that reduces O_2 to H_2O as source of energy. The O_2 reduction process in CcO generates a pH gradient across the bilayer membrane, which provides the driving force for ATP synthesis. The bimetallic active site of CcO has a heme ligated to the protein by a proximal histidine ligand and a distal Cu_B site coordinated by 3 histidine ligands (Fig. 1) (3). In addition to the bimetallic site, there is a conserved tyrosine ligand covalently attached to one of the histidines coordinated to Cu_B (4, 5). The NORs are the older member of the family and are found in bacteria using NO_3^- as source of energy instead of O_2 (2, 6, 7). Although there are no high-resolution crystal structures of NOR, biochemical studies and computer modeling indicate that these enzymes have a histidine-ligated heme, quite like the CcOs, and a distal Fe_B, unlike Cu_B in CcO, coordinated by 3 histidines (Fig. 1) (8–10). NORs do not have the conserved tyrosine residue of CcO but have a few conserved key glutamate residues (11, 12). Although the NOR enzymes are proposed to have specific proton channels, they are probably not involved in generating proton gradients (13–16).

These 2 enzymes exhibit complementary reactivity toward 2 very significant diatomic molecules in nature; O_2 and NO. In eukaryotes CcO (aa_3 type) reduces O_2 to H_2O and is reversibly but strongly inhibited by NO (17–20). Several other CcOs (ba_3, caa_3, cbb_3) are reported to exhibit limited (<1%) NOR activity, i.e., reduce NO to N_2O (7, 21). On the other hand, NORs that reduce NO to N_2O are reversibly but strongly inhibited by O_2, and some of them show modest (≈10%) O_2 reduction activity (12). The parallels in their reactivities toward O_2 and NO and similarities in their secondary structures have led to a hypotheses regarding NOR's and CcO's similar evolutionary origins (6, 22).

Electrochemistry is a very powerful technique that can provide fundamental insights into reaction mechanisms of redox catalysts (23–27). Conventionally, a catalyst is deposited on a conducting electrode material (e.g., graphite); however, this approach does not allow site isolation of the catalysts. Alternatively, catalysts can be covalently attached onto electrode surfaces by taking advantage of self-assembled thiol monolayer formation on gold (Au) surfaces (28–30). This has been achieved by either covalently attaching a thiol tail to the catalyst and then coabsorbing it on a Au substrate (30) or by attaching an alkyne functionality onto the catalyst and then attaching it onto an azide-terminated thiol, absorbed onto Au, by using Cu(I) catalyzed "click" chemistry (Fig. 2) (31–34).

Rotating ring disc electrochemistry (RRDE) provides additional prowess by detecting products or byproducts (35, 36). In this technique, a ring (Pt or Au) is held at a potential where it specifically oxidizes/reduces the product/byproduct of the electrocatalytic reaction occurring on the Au disc electrode it encircles. A common application has been detection of partially reduced oxygen species (PROS) like superoxide (O_2^-) or hydrogen peroxide (H_2O_2) leaked during electrocatalytic reduction of O_2 (32, 37–39). However, this technique has limited collection efficiencies (CE, i.e., percentage of the PROS generated being detected on the ring). Interdigitated array (IDA) Electrodes provide an alternative to rotating ring disc techniques for detecting products/byproducts of unstirred electrochemical reactions (40). IDAs have 2 sets of alternate arrays of electrodes (10 μm wide) spaced 5–10 μm apart (Fig. 2). One set of electrodes has the catalyst immobilized on them whereas the other set has electrodeposited Pt metal and acts as the collector (Fig. 2). The proximity of the collector electrode enables collection efficiencies >55% providing superior sensitivity for PROS detection (41, 42).

In the past, we have reported several functional synthetic model complexes of CcO (32, 39). These functional FeCu CcO models provided insights into important issues such as reversible inhibition by NO and CN^- poisoning (43). Recently, we reported that a bis-ferrous model can also function as an NOR (44). In this article, we investigate the reactivity of a fully reduced NOR model toward O_2 under both steady-state (electrochemically) and single-turnover conditions. Our results show that a bis-ferrous model reduces oxygen efficiently. Reaction of O_2 with this fully reduced catalyst results in the initial formation of a peroxide intermediate, which subsequently undergoes a homolytic O—O bond cleavage resulting in the formation of a bis-ferryl intermediate. This intermediate is very reactive and either can be electrochemically reduced or can perform double oxygenation of a reactive substrate.

Results

Electrochemistry. By using IDA electrodes, the reduction of dioxygen by the bis-iron complexes was studied under (*i*) fast electron flux (500 s^{-1}) (33) by using an 11-azido-undecanethiol with octanethiol as a diluent and (*ii*) slow electron flux (1 s^{-1}) (33) by using an 18-azido-octadecanethiol with hexadecanethiol as a diluent. In a typical experiment, the catalyst was "clicked" onto an Au electrode with a mixed SAM deposited on it (31). To maintain site isolation the concentration of the azido thiol was maintained <10% so that <10% of the resultant SAM surface was covered with the catalyst. Then linear sweeps were per-

Author contributions: J.P.C. and A.D. designed research; A.D., Y.Y., S.G., and R.A.D. performed research; A.D. and Y.Y. analyzed data; and A.D. wrote the paper.

The authors declare no conflict of interest.

[1]To whom correspondence should be addressed. E-mail: jpc@stanford.edu.

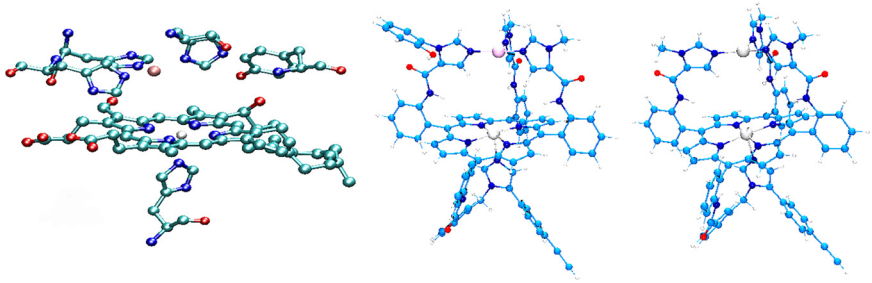

Fig. 1. Active site of CcO [Fe, white; Cu, pink; O, red; C, light blue; and N, dark blue showing the heme, the distal Cu_B, and the conserved Tyr-244 (*Left*), functional CcO model complex (*Center*) with the heme, Cu_B, and tyrosine mimic and the FeFe functional NOR model complex (*Right*) with the heme and Fe_B. Both the FeCuPhOH and the FeFe model have an alkyne functionality appended to them.

formed from +600 mV to −300 mV vs. NHE at 20 mV/s while the Pt collector electrode was held at +900 mV where it oxidizes both O_2^- and H_2O_2 (2 possible PROS) to O_2 (37).

Fig. 3*A* shows a CV of the Fe catalyst in air-saturated buffer (full line) and the corresponding collector current (dashed line). The amount of PROS collected is 11 ± 1% (Table 1), i.e., 89% of the O_2 is reduced to H_2O (45). The selectivity is significantly better with the FeCuPhOH catalyst, which shows only 6 ± 1% PROS (Table 1), i.e., 94% selectivity. This is consistent with previous results obtained from RRDE (32). The PROS formed by using the FeFe (Fig. 3*B*) is only 3 ± 1% (Table 1), which is the highest selectivity for O_2 reduction we have obtained in this catalyst series. Thus, both for the FeCuPhOH and the FeFe catalyst, which possesses additional redox centers (Cu_B and phenol in FeCuPhOH and Fe_B in FeFe), the PROS are reduced relative to the Fe-only catalyst.

Under slow electron flux (1 s^{-1}) the Fe-only catalyst (Table 1) generates 20 ± 2% PROS (Fig. 3*C*). This large increase in PROS indicates an enhanced rate of hydrolysis of the initial Fe^{III}-O_2^- adduct under a slow rate of electron transfer. By using the FeCuPhOH catalyst, the PROS goes down to 6 ± 2% (Table 1) under slow electron transfer. This remarkable reduction of PROS by this catalyst has been reported before by using a rotating ring disc (RRD) assembly and is due to the presence of the distal Cu and the redox-active phenol in the catalyst. Recently, we have shown that on an IDA electrode, the FeCuPhOH catalyst gives the same result as the RRD electrode (45). The FeFe catalyst also shows only 6 ± 2% (Table 1) PROS (Fig. 3*D*), a value similar to the FeCuPhOH catalyst and much less than the Fe catalyst.

Spectroscopy. The resonance Raman (rR) of the bis-ferrous catalyst exposed to O_2 at −80 °C in dichloromethane (CH_2Cl_2) solvent shows a shift of the υ_4 band from 1,357.5 cm^{-1} characteristic of Fe^{II} (Fig. 4*A*, black line) to 1,368 cm^{-1}(Fig. 4*A*, blue line). This is indicative of oxidation of the Fe^{II} heme to a Fe^{III} in this intermediate (46, 47). The data in the lower frequency region show 2 bands that are sensitive to isotopic substitution of O_2. One band is at 822 cm^{-1} and the other is at 583 cm^{-1}; the bands are shifted by 52 cm^{-1} and 32 cm^{-1}, respectively, on O^{18} isotopic substitution. These vibrational data indicate the presence of a heme ferric peroxide species. The υ_4 band at 1,368 cm^{-1} and υ_2 band at 1,568 cm^{-1} are consistent with a low-spin 6-coordinate Fe^{III}-heme (46). Thus, 1 of the 2 electrons needed to reduce O_2 to peroxide is derived from the heme, and hence, the other must be derived from Fe_B. This species could be either an end-on or side-on peroxide. Although no Fe_B-O vibration could be observed in the rR, the high O—O, single Fe-O vibration and the low-spin state of the heme (requiring a strong ligand field) are consistent with an end-on peroxide rather than a side-on peroxide (48, 49).

Upon warming the temperature to −20 °C, the υ_4 band moves to 1,373.7 cm^{-1}, and the υ_2 band shifts to 1,572.1 cm^{-1}. Such high-energy υ_4 and υ_2 bands are characteristic of ferryl species

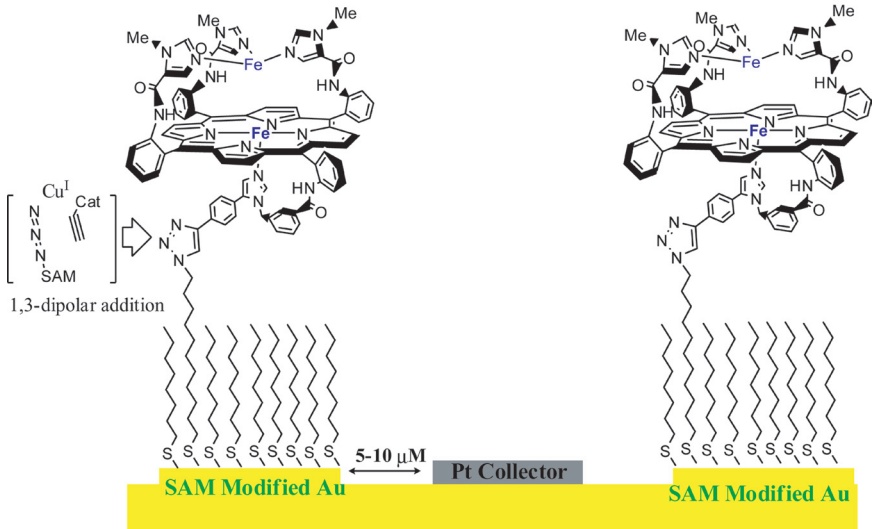

Fig. 2. Modifying IDAs with catalyst by using Cu(I) catalyzed 1,3-dipolar addition of an azide to an alkyne (i.e., ''click'' reaction). The Pt collector electrode is spaced 5–10 μM away from this electrode, which allows higher collection efficiencies.

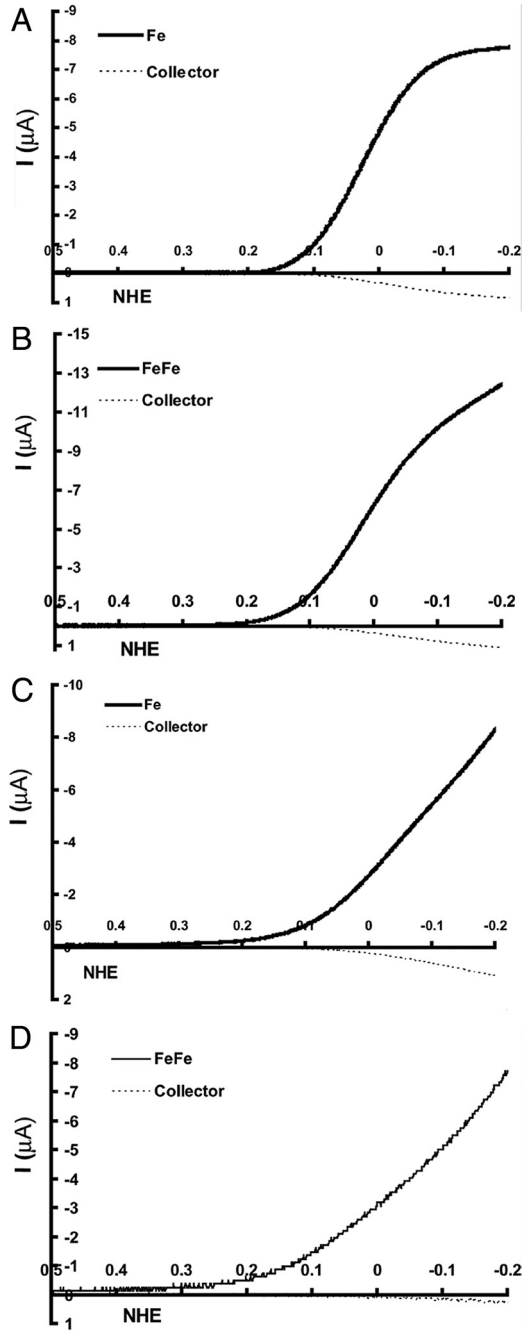

Fig. 3. Electrocatalytic O_2 reduction current (in black) vs. Pt collector current (dashed black) for fast (*A* and *B*) and slow (*C* and *D*) SAM.

(50, 51). The low-energy data on this species show 2 bands that are oxygen isotope sensitive. One band is observed at 808 cm^{-1}, and the other is observed at 756 cm^{-1}; the bands shift by 32 cm^{-1}

Table 1. Summary of PROS obtained by using IDA

	PROS	
Model	Fast, %	Slow, %
Fe	11 ± 2	20 ± 2
FeCuPhOH	6 ± 1	6 ± 1
FeFe	3 ± 1	6 ± 2

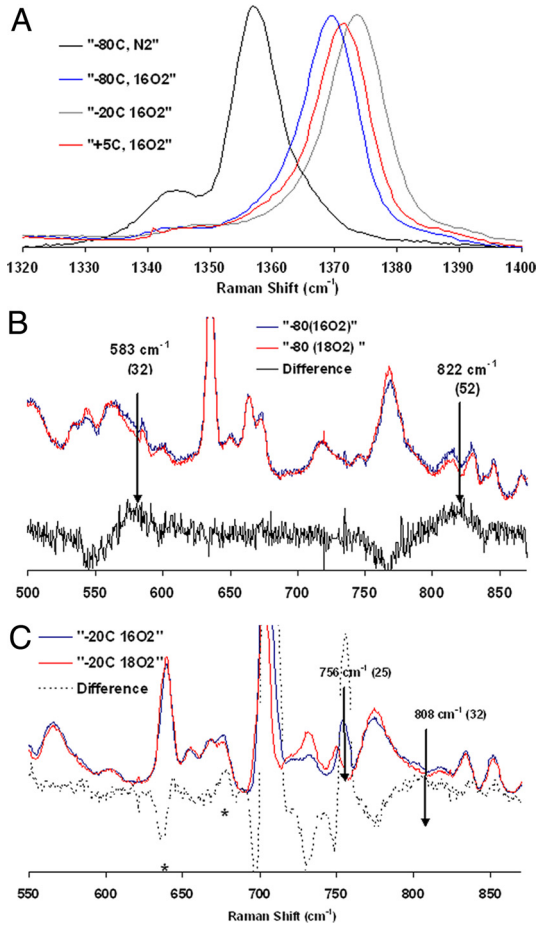

Fig. 4. rR data obtained with 424-nm excitation, 15-mW power. (*A*) Data at the high-energy region for the species involved. (*B*) Low-energy data obtained for sample quenched after addition oxygen at −80 °C. (*C*) Low-energy data obtained for sample quenched after warming the −80 °C sample to −20 °C. The features at 630 cm^{-1} and 676 cm^{-1} in the difference spectrum of the −20 °C sample arise from porphyrin bands of the final decay product.

and 25 cm^{-1}, respectively. Fe-O vibrations for Fe^{IV}═O porphyrin species have been observed between 745 cm^{-1} and 850 cm^{-1} (51, 52), and those for nonheme ferryl species are observed between 800 and 840 cm^{-1} depending on spin state and different *trans* ligands (53–56). The presence of only these 2 oxygen isotope-sensitive bands at 756 cm^{-1} and 808 cm^{-1} indicate that there are 2 distinct ferryl species in this intermediate. These could arise from a *trans* heme/nonheme bis-ferryl intermediate that would result from the homolytic cleavage of the O—O bond in the initial peroxide intermediate. These could also arise from 2 heme ferryl species that differ in Fe-O bonding. However, the single set of υ_4 and υ_2 porphyrin bands indicate the presence of a single ferryl heme species. The possibility of a *trans* heme/nonheme bis-ferryl species is evaluated below. Upon further warming, the reaction to 5 °C the υ_4 band shifts to 1,371.6 cm^{-1}, the υ_2 shifts to 1,570 cm^{-1} (Scheme 1), and the isotope-sensitive ferryl bands lose all of their intensity. This indicates decay of both the ferryl species and formation of a low-spin Fe^{III} heme species (46).

The rR data on the intermediates cryogenically trapped during the single-turnover experiment described above indicates the possible involvement of a *trans* heme/nonheme bis-ferryl species from reaction of the bis-ferrous catalyst with O_2. To provide further evidence for the presence of such species, we evaluated their oxo transfer reactivity using triphenylphosphine,

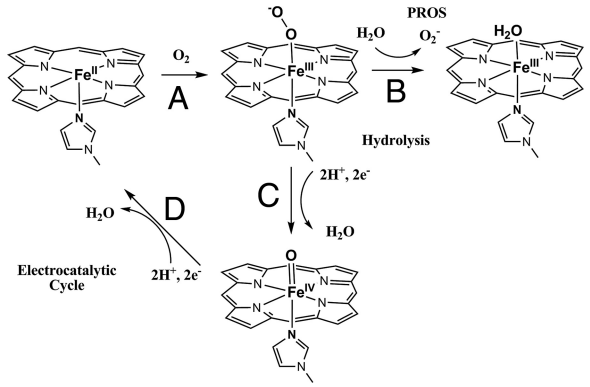

Scheme 1. Schematic representation of the steps involved in O_2 reduction (electrocatalytic cycle) by using a Fe-only porphyrin as well as generation of PROS (via hydrolysis).

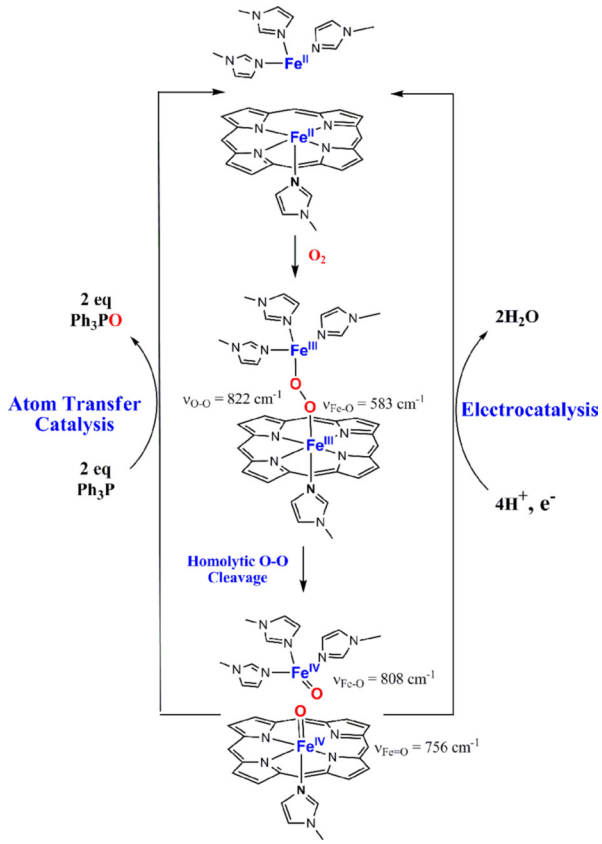

Scheme 2. Proposed mechanism for the reaction of O_2 with the bis-ferrous functional NOR model.

which can be oxidized to triphenylphosphine oxide by both heme and nonheme ferryl species (57–59). GC analysis of a reaction of O_2 with the bis-ferrous catalyst in presence of triphenylphosphine indicates formation of 5–6 equivalents of triphenylphosphine oxide. Because there are no additional reductants present under the reaction conditions, this indicates that the reaction is catalytic and shows 2–3 turnovers. Thus, this implies that, indeed, a heme/nonheme *trans* bis-ferryl intermediate is formed resulting from the reaction of the bis-ferrous complex with O_2. Each of the ferryl species donates an oxygen atom to a molecule of triphenyl phosphine, resulting in regeneration of the bis-ferrous form (Scheme 1). This makes the reaction catalytic and 2 to 3 turnovers were obtained per catalyst. Further exploration of this reactivity remains to be completed.

Discussion

In this article, we described O_2 reduction by a bis-ferrous model, which shows NOR activity. Our electrochemical data indicate that this catalyst can perform efficient 4e reduction of O_2 with negligible PROS formation. Under slow electron flux, the 95% selectivity for 4e O_2 reduction (i.e., 5% production of H_2O_2) is comparable with the FeCuPhOH catalyst previously reported and is much greater than an Fe-only catalyst, which shows as much as 20 ± 2% PROS, i.e., 20% H_2O_2 production. The primary mechanism by which PROS are produced during electrocatalytic O_2 reduction is proposed to be the hydrolysis of the initial Fe-O_2 adduct formed (step B, Scheme 1) (60). This leads to the generation of O_2^-, which would be detected either by itself or as H_2O_2 resulting from its disproportionation. In the absence of additional redox-active centers, the O—O bond cleavage by the Fe-only catalyst (which does not have the necessary 4e's to reduce O_2 to H_2O) can be limited by electron flux arriving from the electrode (step C, Scheme 1). This is why the 11 ± 1% PROS the Fe-only catalyst produced under fast electron flux (500 s^{-1}) increases dramatically to 20 ± 2% under slow (1 s^{-1}) electron flux. However, the FeFe catalyst possesses all 4 electrons necessary for O_2 reduction (2 from each Fe), and thus it does not produce significant PROS either under fast or slow electron transfer conditions because the O—O bond fission generating the ferryl species precedes hydrolysis of the oxy species; i.e., step C is much faster than step B in Scheme 1. This is indeed the case as we were able to trap and identify the *trans* heme/nonheme bis-ferryl intermediate by using rR spectroscopy.

Two distinct intermediates were trapped and characterized by using rR spectroscopy under single-turnover conditions. The vibrational characteristics of the first intermediate are consistent with a Fe^{III}-heme peroxide species with $\upsilon_{O—O}$ at 822 cm^{-1} and υ_{Fe-O} at 583 cm^{-1}. On warming the sample to −20 °C a *trans* heme/nonheme bis-ferryl intermediate is formed resulting from a homolytic O—O bond cleavage. The 2 Fe-O vibrations are observed at 808 cm^{-1} (nonheme) and 756 cm^{-1} (heme), which are within the expected range of Fe-O vibrations for heme and nonheme ferryl species. From the relative enhancements of the 2 ferryl modes via excitation into the porphyrin soret band, we believe that the strongly enhanced 756 cm^{-1} mode corresponds to the heme ferryl species, whereas the weakly enhanced 808-cm^{-1} mode corresponds to the nonheme ferryl species. The Fe-O vibration for the heme ferryl species is on the lower side of the range reported for heme ferryl species (51). These values are very similar to those reported for lactoperoxidase (745 cm^{-1}) and cytochrome *c* peroxidases (753 cm^{-1}) (52) and may indicate weakening of the Fe^{IV}═O bond by hydrogen bonding or a strong *trans* effect of the covalently attached proximal imidazole tail (52).

The occurrence of the bis-ferryl intermediate after a peroxide intermediate indicates a homolytic O—O bond cleavage occurring in this complex. Alternatively, a heterolytic O—O bond cleavage would result in the formation of a compound I species and a Fe_B^{III}. Such a species would be expected to have a very weak and low-energy υ_4 vibration inconsistent with the rR data observed for this intermediate. A homolytic O—O bond cleavage may also result in the formation of a bridging bis-μ-oxo $Fe^{IV}Fe^{IV}$ species similar to those proposed for methane monooxygenase active site. Although there is no precedent of such a complex that would allow a direct comparison of its spectroscopic features to the one presented here, such an intermediate cannot perform 2 oxygen transfer reactions because 1 oxygen transfer reaction would result in the formation of a μ-oxo $Fe^{III}Fe^{III}$ species that is not capable of an additional oxo atom transfer as was observed here. These considerations lead to the

mechanistic proposal of O_2 reduction by the bis-iron complex presented in Scheme 2. The bis-ferrous complex binds O_2 to form an end-on bridging peroxide. This undergoes a homolytic O—O bond cleavage to generate a *trans* heme/nonheme bis ferryl intermediate. This species is reduced to the bis ferrous form either by $4e^-$ transfers from the electrode during electrocatalysis or via oxygen atom transfers to 2 equivalents of triphenylphosphine during atom transfer catalysis.

In summary, our results indicate that a FeFe active site of NOR can be as efficient in O_2 reduction as a CcO active site. The high-valent intermediates involved in CcOs have only 1 ferryl center (both P_R and P_M) (1). However, O_2 reduction by a NOR site could possibly result in a *trans* heme/nonheme bis-ferryl intermediate. The presence of such a reactive intermediate could be disadvantageous because it might lead to degradation of the enzyme active site under conditions of slow electron flux (i.e., if these species are not rapidly reduced). These results imply that these NOR model sites may be potential dioxygenases and opens up routes for future research in this fundamentally important area.

Materials and Methods

All chemicals obtained commercially were used without further purification. The synthesis of the FeFe catalyst has been reported before (44). O^{18}-enriched O_2 (>95% enrichment) was purchased from Cambridge Isotopes. The solvents used were purified in a solvent still before moving them in a N_2 glove box, where the solutions of the reduced catalysts were prepared.

Interdigitated electrodes were obtained from the Stanford nanofabrication facility. Pt was electrodeposited on 1 set of alternate array electrodes from a solution of K_2PtCl_4. The Pt electrode was cleaned before experiments by several CV cycles between 1,600 and −300 mV in pH 7 buffer or 0.5 M H_2SO_4. The Au electrode was also electrochemically cleaned before experiments by several CV cycles between 1,650 and −200 mV at 250 mV in 0.5 H_2SO_4. The azide-terminated thiols were synthesized and characterized as reported previously (33, 45). The mixed thiol monolayer was deposited by immersing the cleaned IDAs in a 0.4 mM solution of a mixture of azide-terminated thiol and thiols in ethanol for 1 h.

The alkyne-terminated catalysts were covalently attached onto the azide-terminated thiol monolayer by using Cu(I) catalyzed 1,3-dipolar cyclo-addition reaction (61). A solution containing 10–20 μM catalyst, 20 μM Cu(II)TBTA, and 100 μM sodium ascorbate in a 3:2 mixture of DMSO and water was placed over the SAM-modified electrodes in a N_2 glove box. The coverage of the catalyst was maintained between 1% and 10% and was measured by integrating the charge under an anaerobic CV or an aerobic CV with 100 mM imidazole (which inhibits O_2 reduction). All electrochemical measurements were performed at room temperature (≈21 °C) at pH 7 phosphate buffer with 100 mM KPF_6 electrolyte on a commercially purchased Pine AFCBP1 bipotentiostat (Pine Instruments). The PROS were determined by collection scans that were run at 20 mV. To measure the collection efficiency of the IDA's linear sweep of a set of Au electrodes were performed between 500 and −600 mV while the collector Pt electrode was held at a constant potential of 900 mV vs. NHE. At this potential, the Pt electrode oxidizes both O_2^- and H_2O_2 (back to O_2) produced due to quantitative 2e reduction of O_2 by Au at pH 7 (32). The ratio of the electrocatalytic current at the Au electrode and that registered by the Pt at 100–0 mV vs. NHE is the collection efficiency of the IDA. Typical values range from 55% to 60% i.e., 55–60% of the PROS produced at the Au electrode is detected in the adjacent Pt electrode before diffusion into bulk solution. PROS generated by the catalysts are quantified by the percentage of the current detected by the Pt electrode during steady-state O_2 reduction of O_2 by the catalyst clicked onto the adjacent SAM-coated Au electrode corrected for collection efficiency of that IDA (determined before SAM formation).

For spectroscopic measurements, O_2 is added to the bis-ferrous catalyst at −80 °C. The solution is kept at −80 °C for 20–30 min before spectroscopic measurements or warming it up to −20 °C or room temperature. Resonance Raman spectra were obtained by using an Andor Newton electronically cooled CCD detector on a Spex 1877 CP triple monochromator with 1,800 and 2,400 grooves per millimeter holographic spectrograph gratings. Excitation was provided by a Dye Laser (Stilbene; Coherent 599) that was energized by a Coherent Innova Sabre 25/7 Ar^+ CW ion laser. The laser line 425 nm (≈10–20 mW) was used for excitation. The spectral resolution was <2 cm^{-1}. Sample concentrations were ≈1–2 mM in Fe. The samples were either cooled to 77 K in a quartz liquid nitrogen finger dewar (Wilmad) and hand spun to minimize sample decomposition during scan collection. No sample degradation or photochemical dissociation were observed in any of these experiments. The Raman shifts were calibrated by using the nonresonance scattering from solid citric acid.

Conditions for Quantifying Oxo Transfer Reactivity. A solution of Fe-only catalyst in dichloromethane (2 mM, 10 μL) was sealed in a vial under nitrogen. It was cooled to −40 °C. A solution of $Fe(OTf)_2$ (2 mM, 10 μL) in dichloromethane was injected. The mixture was kept for 10 min at −40 °C to ensure distal Fe binding. Then a solution of PPh_3 (20 mM, 10 μL) in dichloromethane was added, followed by a saturated O_2 solution in dichloromethane (50 μL). The mixture was kept in the cold bath and allowed to slowly warm to 0 °C (≈1 h). The amount of the remaining triphenylphosphine and the produced triphenylphosphine oxide were analyzed by gas chromatography on a HP 6890 chromatograph. They were quantitatively determined with the use of a known amount of nitrobenzene as an internal standard. The identity of the compounds was confirmed by comparing retention times of the compound with authentic samples. A 30-m × 0.25-mm column of HP (Innowax, 0.25-μm film) on fused silica was used. Triphenylphosphine oxide (2–3%) was observed in parallel control experiments without adding the catalyst before adding oxygen. Helium was used as a carrier gas at a flow rate of 1 mL/min. Column temperature, 250 °C; injector temperature, 260 °C; detector temperature, 260 °C; injection volume, 0.04 μL.

ACKNOWLEDGMENTS. We thank Prof. Edward I Solomon for access to his resonance Raman instrument and Drs. Ali Hosseini and Todd Eberspacher for their help with the interdigitated electrodes. This material is based on work supported by National Institutes of Health Grants GM-69568-01 and GM-17880-38.

1. Ferguson-Miller S, Babcock GT (1996) Heme/copper terminal oxidases. *Chem Rev* 96:2889–2908.
2. Zumft WG (2005) Nitric oxide reductases of prokaryotes with emphasis on the respiratory, heme-copper oxidase type. *J Inorg Biochem* 99:194–215.
3. Yoshikawa S, et al. (1998) Redox-coupled crystal structural changes in bovine heart cytochrome *c* oxidase. *Science* 280:1723–1729.
4. Ostermeier C, Harrenga A, Ermler U, Michel H (1997) Structure at 2.7 A resolution of the *Paracoccus denitrificans* two-subunit cytochrome c oxidase complexed with an antibody F-V fragment. *Proc Natl Acad Sci USA* 94:10547–10553.
5. McCauley KM, Vrtis JM, Dupont J, van der Donk WA (2000) Insights into the functional role of the tyrosine-histidine linkage in cytochrome *c* oxidase. *J Am Chem Soc* 122:2403–2404.
6. Saraste M, Castresana J (1994) Cytochrome oxidase evolved by tinkering with denitrification enzymes. *FEBS Lett* 341:1–4.
7. Pinakoulaki E, Varotsis C (2008) Nitric oxide activation and reduction by heme-copper oxidoreductases and nitric oxide reductase. *J Inorg Biochem* 102:1277–1287.
8. Hendriks J, et al. (1998) The active site of the bacterial nitric oxide reductase is a dinuclear iron center. *Biochemistry* 37:13102–13109.
9. Groenberg KLC, et al. (1999) A low-redox potential heme in the dinuclear center of bacterial nitric oxide reductase: Implications for the evolution of energy-conserving heme-copper oxidases. *Biochemistry* 38:13780–13786.
10. Zumft WG, Braun C, Cuypers H (1994) Nitric oxide reductase from *Pseudomonas stutzeri*. Primary structure and gene organization of a novel bacterial cytochrome *bc* complex. *Eur J Biochem* 219:481–490.
11. Thorndycroft FH, Butland G, Richardson DJ, Watmough NJ (2007) A new assay for nitric oxide reductase reveals two conserved glutamate residues form the entrance to a proton-conducting channel in the bacterial enzyme. *Biochem J* 401:111–119.
12. Butland G, Spiro S, Watmough NJ, Richardson DJ (2001) Two conserved glutamates in the bacterial nitric oxide reductase are essential for activity but not assembly of the enzyme. *J Bacteriol* 183:189–199.
13. Hendriks JHM, Jasaitis A, Saraste M, Verkhovsky MI (2002) Proton and electron pathways in the bacterial nitric oxide reductase. *Biochemistry* 41:2331–2340.
14. Flock U, Watmough NJ, Aedelroth P (2005) Electron/proton coupling in bacterial nitric oxide reductase during reduction of oxygen. *Biochemistry* 44:10711–10719.
15. Flock U, Reimann J, Aedelroth P (2006) Proton transfer in bacterial nitric oxide reductase. *Biochem Soc Trans* 34:188–190.
16. Flock U, et al. (2008) Defining the proton entry point in the bacterial respiratory nitric-oxide reductase. *J Biol Chem* 283:3839–3845.
17. Brudvig GW, Stevens TH, Chan SI (1980) Reactions of nitric oxide with cytochrome *c* oxidase. *Biochemistry* 19:5275–5285.
18. Parihar A, Vaccaro P, Ghafourifar P (2008) Nitric oxide irreversibly inhibits cytochrome oxidase at low oxygen concentrations: Evidence for inverse oxygen concentration-dependent peroxynitrite formation. *IUBMB Life* 60:64–67.
19. Petersen L (1977) The effect of inhibitors on the oxygen kinetics of cytochrome *c* oxidase. *Biocheim Biophys Acta* 460:299–307.
20. Brunori M, et al. (2006) Nitric oxide and the respiratory enzyme. *Biochim Biophys* Acta 1757:1144–1154.

21. Giuffrè A, et al. (1999) The heme-copper oxidases of *Thermus thermophilus* catalyze the reduction of nitric oxide: Evolutionary implications. *Proc Natl Acad Sci USA* 96:14718–14723.
22. van der Oost J, et al. (1994) The heme-copper oxidase family consists of three distinct types of terminal oxidases and is related to nitric oxide reductase. *FEMS Microbiol Lett* 121:1–10.
23. Cracknell JA, Vincent KA, Armstrong FA (2008) Enzymes as working or inspirational electrocatalysts for fuel cells and electrolysis. *Chem Rev* 108:2439–2461.
24. De Lacey AL, Fernandez VM, Rousset M, Cammack R (2007) Activation and inactivation of hydrogenase function and the catalytic cycle: spectroelectrochemical studies. *Chem Rev* 107:4304–4330.
25. Jutand A (2008) Contribution of electrochemistry to organometallic catalysis. *Chem Rev* 108:2300–2347.
26. Saveant J-M (2008) Molecular catalysis of electrochemical reactions. Mechanistic aspects. *Chem Rev* 108:2348–2378.
27. Saveant JM (1980) Catalysis of chemical reactions by electrodes. *Acc Chem Res* 13:323–329.
28. Ulman A (1996) Formation and structure of self-assembled monolayers. *Chem Rev* 96:1533–1554.
29. Prime KL, Whitesides GM (1991) Self-assembled organic monolayers: Model systems for studying adsorption of proteins at surfaces. *Science* 252:1164–1167.
30. Peck SR, et al. (1995) Voltammetry of self-assembled ferroceneoctanethiol monolayers on metal-coated high-temperature superconductor electrodes at sub-Tc temperatures. *J Am Chem Soc* 117:1121–1126.
31. Collman JP, Devaraj NK, Chidsey CED (2004) ''Clicking'' functionality onto electrode surfaces. *Langmuir* 20:1051–1053.
32. Collman JP, et al. (2007) A cytochrome *c* oxidase model catalyzes oxygen to water reduction under rate-limiting electron flux. *Science* 315:1565–1568.
33. Collman JP, Devaraj NK, Eberspacher TPA, Chidsey CED (2006) Mixed azide-terminated monolayers: A platform for modifying electrode surfaces. *Langmuir* 22:2457–2464.
34. Collman JP, et al. (1996) Electrocatalytic reduction of dioxygen by diruthenium cofacial diporphyrins axially-bound to a gold-supported, self-assembled monolayer *Inorg Chem* 35:1751–1752.
35. Myuller L, Nekrasov L (1964) Electrochemical reduction of oxygen on platinum by the rotating disk electrode with a ring. *Electrochim Acta* 9:1015–1023.
36. Geiger T, Anson FC (1980) Rotating ring-disk electrode with demountable disk. *Anal Chem* 52:2448–2450.
37. Shigehara K, Anson FC (1982) Electrocatalytic activity of three iron porphyrins in the reduction of dioxygen and hydrogen peroxide at graphite cathodes. *J Phys Chem* 86:2776–2783.
38. Collman JP, et al. (1980) Electrode catalysis of the four-electron reduction of oxygen to water by dicobalt face-to-face porphyrins. *J Am Chem Soc* 102:6027–6036.
39. Collman JP, Boulatov R, Sunderland CJ, Fu L (2004) Functional analogues of cytochrome *c* oxidase, myoglobin, and hemoglobin. *Chem Rev* 104:561–588.
40. Chidsey CE, Feldman BJ, Lundgren C, Murray RW (1986) Micrometer-spaced platinum interdigitated array electrode: Fabrication, theory, and initial use. *Anal Chem* 58:601–607.
41. Hutchison JE, Postlethwaite TA, Murray RW (1993) Molecular films of thiol-derivatized tetraphenylporphyrins on gold: Film formation and electrocatalytic dioxygen reduction. *Langmuir* 9:3277–3283.
42. Postlethwaite TA, et al. (1996) Interdigitated array electrode as an alternative to the rotated ring-disk electrode for determination of the reaction products of dioxygen reduction. *Anal Chem* 68:2951–2958.
43. Collman JP, et al. (2008) Interaction of nitric oxide with a functional model of cytochrome *c* oxidase. *Proc Natl Acad Sci USA* 105:9892–9896.
44. Collman JP, et al. (2008) A functional nitric oxide reductase model. *Proc Natl Acad Sci USA* 105:15660–15665.
45. Collman JP, et al. (2009) Role of a distal water cluster in the catalytic O_2 reduction by cytochrome *c* oxidase models immobilized on interdigitated array electrodes. *Proc Natl Acad Sci USA* 106:7320–7323.
46. Burke JM, et al. (1978) Structure-sensitive resonance Raman bands of tetraphenyl and ''picket fence'' porphyrin–iron complexes, including an oxyhemoglobin analog. *J Am Chem Soc* 100:6083–6088.
47. Spiro TG, Strekas C (1974) Resonance Raman spectra of heme proteins effects of oxidation and spin state. *J Am Chem Soc* 96:338–345.
48. Chishiro T, et al. (2003) Isolation and crystal structure of a peroxo-bridged heme–copper complex *Angew Chem Int Ed* 42:2788–2791.
49. Kim E, et al. (2004) Heme/Cu/O_2 Reactivity: Change in FeIII(O_2)CuII unit peroxo binding geometry effected by tridentate copper chelation. *J Am Chem Soc* 126:12716–12717.
50. Mizutani Y, Hashimoto S, Tatsuno Y, Kitagawa T (1990) Resonance Raman pursuit of the change from iron(II)-oxygen (FeII-O2) to iron(III)-hydrohxyl (FeIII-OH) via iron(IV):oxygen (FeIV:O) in the autoxidation of ferrous iron-porphyrin. *J Am Chem Soc* 112:6809–6814.
51. Oertling WA, Kean RT, Wever R, Babcock GT (1990) Factors affecting the iron–oxygen vibrations of ferrous oxy and ferryl oxo heme proteins and model compounds. *Inorg Chem* 29:2633–2645.
52. Reczek CM, Sitter AJ, Terner J (1989) Resonance Raman characterization of heme iron(IV)=oxygen groups of intermediates of yeast cytochrome *c* peroxidase and lactoperoxidase. *J Mol Struct* 214:27–41.
53. Green MT (2006) Application of Badger's Rule to heme and non-heme iron-oxygen bonds: An examination of ferryl protonation states. *J Am Chem Soc* 128:1902–1906.
54. Krebs C, Fujimori DG, Walsh CT, Bollinger JM, Jr (2007) Non-heme Fe(IV)-oxo intermediates *Acc Chem Res* 40:484–492.
55. Sastri CV, et al. (2005) Axial ligand substituted nonheme FeIV:O complexes: Observation of near-UV LMCT bands and Fe:O Raman vibrations. *J Am Chem Soc* 127:12494–12495.
56. Jackson TA, et al. (2008) Axial ligand effects on the geometric and electronic structures of nonheme oxoiron(IV) complexes. *J Am Chem Soc* 130:12394–12407.
57. Que L (2007) The road to non-heme oxoferryls and beyond. *Acc Chem Res* 40:493–500.
58. Rohde J-U, et al. (2003) Crystallographic and spectroscopic characterization of a nonheme Fe(IV)=O complex. *Science* 299:1037–1039.
59. Collman JP, et al. (2007) Intramolecular single-turnover reaction in a cytochrome *c* oxidase model bearing a Tyr244 mimic. *J Am Chem Soc* 129:5794–5795.
60. Boulatov RC, Shiryaeva JP, Sunderland IM, Christopher J (2002) Functional analogues of the dioxygen reduction site in cytochrome oxidase: Mechanistic aspects and possible effects of CuB. *J Am Chem Soc* 124:11923–11935.
61. Kolb HC, Finn MG, Sharpless KB (2001) Click chemistry: Diverse chemical function from a few good reactions. *Angew Chem Int Ed* 40:2004–2021.